Available online at www.sciencedirect.com
SCIENCE DIRECT®
Journal of Solid State Chemistry 178 (2005) 976–988
JOURNAL OF SOLID STATE CHEMISTRY
www.elsevier.com/locate/jssc

Oxonitridosilicate chlorides—synthesis, single-crystal X-ray and neutron powder diffraction, chemical analysis and properties of $Ln_4[Si_4O_{3+x}N_{7-x}]Cl_{1-x}O_x$ with Ln = Ce, Pr, Nd and $x \approx 0.2$

Alexandra Lieb[a], Mark T. Weller[b], Paul F. Henry[b,1], Rainer Niewa[c], Rainer Pöttgen[d], Rolf-Dieter Hoffmann[d], Heidi E. Höfer[e], Wolfgang Schnick[a,*]

[a]Department Chemie und Biochemie, Ludwig-Maximilians-Universität München, Butenandtstraße 5-13 (D), D-81377 München, Germany
[b]Department of Chemistry, University of Southampton, Highfield, Southampton SO17 1BJ, UK
[c]Max Planck Institut für Chemische Physik fester Stoffe, Nöthnitzer Straße 40, D-01187 Dresden, Germany
[d]Institut für Anorganische und Analytische Chemie, Westfälische Wilhelms-Universität Münster, Corrensstraße 36, D-48149 Münster, Germany
[e]Institut für Mineralogie, Abteilung Petrologie und Geochemie, J.W. Goethe Universität Frankfurt, Senckenberganlage 28, D-60325 Frankfurt am Main, Germany

Received 16 September 2004; received in revised form 16 September 2004; accepted 14 October 2004

Abstract

The isotypic oxonitridosilicate chlorides $Ln_4[Si_4O_{3+x}N_{7-x}]Cl_{1-x}O_x$ with Ln = Ce, Pr, Nd and $x \approx 0.2$ were obtained by the reaction of the respective rare-earth metals, their oxides and chlorides with "$Si(NH)_2$" in a radiofrequency furnace at temperatures around 1800 °C, using CsCl as a flux. The crystal structures were determined by single-crystal X-ray diffraction ($P2_13$, no. 198, $Z = 4$, Ce: $a = 10.4461(12)$ pm, $R1 = 0.0524$; Pr: $a = 10.3720(12)$ pm, $R1 = 0.0415$; Nd: $a = 10.3618(12)$ pm, $R1 = 0.0257$) and found to be isotypic with $Ce_4[Si_4O_4N_6]O$. In order to characterize the incorporation of chlorine into the structure, the crystallographic site occupation factors of O, N and Cl were determined by neutron powder diffraction. Furthermore, these results were substantiated by the chemical analyses for $Pr_4[Si_4O_{3+x}N_{7-x}]Cl_{1-x}O_x$ and electron microprobe analyses for all of the synthesized oxonitridosilicate chlorides. Temperature-dependent magnetic susceptibility measurements of the cerium and the praseodymium compound indicate Curie–Weiss behavior with experimentally determined magnetic moments of 2.15(5) μ_B/Ce and 3.50(5) μ_B/Pr, respectively. No magnetic ordering could be detected down to 2 K. The $4f^1$ of cerium has been confirmed by XAS measurements.

Keywords: Cerium; Praseodymium; Neodymium; Chloride; Oxonitridosilicate; Crystal structure; Neutron diffraction; Magnetism; X-ray spectroscopy; Light element electron probe microanalyses

1. Introduction

Nitridosilicates derive from the classical oxosilicates by a formal exchange of oxygen by nitrogen, whereby the SiO_4 tetrahedra become SiN_4 tetrahedra. This substitution results in a significant extension of the structural possibilities [1,2]. Oxonitridosilicates (so-called "sions") represent an intermediate class of compounds between oxosilicates and oxonitridosilicates. They are of considerable interest for the development of inorganic materials for high-performance applications owing to their structural diversity and their material properties (high thermal and chemical stability). In the context of systematic investigations concerning structural peculiarities of that type of compounds

*Corresponding author. Fax: +49 89 2180 77440.
E-mail address: wolfgang.schnick@uni-muenchen.de (W. Schnick).
[1]Current address: Institut Laue-Langevin, 6, rue Jules Horowitz, BP 156-38042 Grenoble Cedex 9, France.

0022-4596/$ - see front matter
doi:10.1016/j.jssc.2004.10.022

we synthesized and investigated the series $Ln_4[Si_4O_{3+x}N_{7-x}]Cl_{1-x}O_x$ (*Ln* = Ce, Pr, Nd), which represent the first oxonitridosilicate chlorides.

These compounds are isotypic with $Ce_4[Si_4O_4N_6]O$ [3], which crystallizes with cubic symmetry ($P2_13$) but represents a layer silicate solely composed of tetrahedra of Q^3 type [4] . This can be explained by a hyperbolically corrugated layer $[Si_4O_4N_6]^{10-}$ enveloping complex $[OCe_4]^{10+}$ cations (Fig. 1). Compounds containing oxygen centered tetrahedral $[OM_4]^{n+}$ cations have been found frequently [5]. For the new compounds it has been assumed that the chlorine atoms partially substitute oxygen atoms, thus building up $[Cl_{1-x}O_xLn_4]^{(11-x)+}$ tetrahedra. But chlorine that is tetrahedrally coordinated by metal atoms only has been observed in binary or ternary metal chlorides such as $NdCl_2$ [6] or $Sr_9Nd_5Cl_{33}$ [7]. Furthermore, such complex cations $[ClM_4]^{11+}$ have been postulated in $Pr_7S_6Cl_9$ and $Nd_7S_6Cl_7$ by reasons of charge neutrality [8]. This resulted in a very careful examination of the oxonitridosilicate chlorides concerning the position and the magnitude of the chlorine substitution.

Additionally, a split position inside the complex cation (concerning *Ln*2/*Ln*3) has been observed in $Ln_4[Si_4O_{3+x}N_{7-x}]Cl_{1-x}O_x$ as in $Ce_4[Si_4O_4N_6]O$, which could be confirmed by DFT calculations [3,9].

In $Ce_4[Si_4O_4N_6]O$, an ordered distribution of O and N within the anionic layer has been found. That cannot be realized in the new compounds owing to the different O/N proportion in the anionic part of the structure, deriving from the postulated substitution of O^{2-} with Cl^- in the complex cation. Thus, one of the points of interest is related to the O/N distribution.

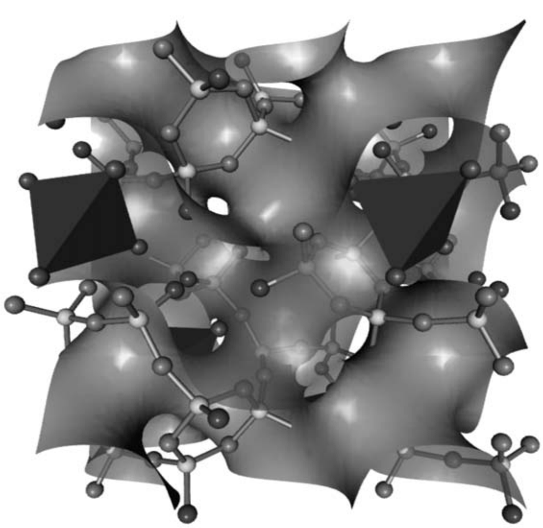

Fig. 1. Hyperbolically layered structure of $Ce_4[Si_4O_4N_6]O$ [3] shown with periodic nodal surface PNS FYxxx, view along [100], Si: light gray circles, N: medium gray circles, O: dark gray circles, Ce atoms are shown as members of black tetrahedra.

In addition, we determined the magnetic properties of the cerium and the praseodymium compound and performed XAS measurements to determine the oxidation state of the cerium atoms in $Ce_4[Si_4O_{3+x}N_{7-x}]Cl_{1-x}O_x$.

2. Experimental

2.1. Syntheses

2.1.1. Synthesis of silicon diimide "Si(NH)$_2$"

Using "Si(NH)$_2$" instead of the relatively unreactive Si_3N_4 as starting material proved to be advantageous for the synthesis of the nitridosilicates and this also holds for the sions and sialons [1,2,10]. "Si(NH)$_2$" was obtained by ammonolysis of $SiCl_4$ followed by a thermal treatment at 600 °C under an atmosphere of pure NH_3 (see Eqs. (1) and (2)). A detailed description of the synthesis of "Si(NH)$_2$" is given in Ref. [9].

$$SiCl_4 + 6\,NH_3 \xrightarrow[NH_3\ \text{atmosphere}]{-78\,^\circ C} \text{“}Si(NH)_2\text{”} + 4\,NH_4Cl, \quad (1)$$

$$\text{“}Si(NH)_2\text{”} + 4\,NH_4Cl \xrightarrow[NH_3\ \text{atmosphere}]{600\,^\circ C,\ -NH_4Cl} \text{“}Si(NH)_2\text{”}. \quad (2)$$

"Si(NH)$_2$" was obtained as an X-ray amorphous and reactive product. It is converted to amorphous Si_3N_4 at temperatures above 900 °C and is an important precursor for the technical production of Si_3N_4 ceramics [11].

2.1.2. Synthesis of $Ln_4[Si_4O_{3+x}N_{7-x}]Cl_{1-x}O_x$ with Ln = Ce, Pr, Nd

Ln = Ce: A mixture of Ce (160 mg/1.14 mmol, Goodfellow, 99.99%, powder), "Si(NH)$_2$" (116 mg/2 mmol), $CeCl_3$ (200 mg/0.81 mmol, Chempur, 99.9%), CeO_2 (60 mg/0.35 mmol, Chempur, 99.99%) and CsCl (1000 mg/6 mmol, Chempur, 99.99%) as a flux was thoroughly mixed and transferred into a tungsten crucible in a glove box (argon atmosphere). The crucible then was positioned in a water-cooled silica glass reactor of a radiofrequency furnace. It was heated under a pure nitrogen atmosphere to 1100 °C within 5 min, then to 1850 °C within 2 h, maintained at that temperature for 1 h and subsequently cooled to 1100 °C within 45 h. Finally, the product was quenched to room temperature. Further details about the experimental setup are given in Ref. [10].

The praseodymium and neodymium compounds were synthesized similarly. *Ln* = Pr: mixture of Pr (160 mg/1.14 mmol, Chempur, 99.9%), "Si(NH)$_2$" (116 mg, 2 mmol), $PrCl_3$ (200 mg/0.81 mmol, Chempur, 99.9%), PrO_2 (60 mg/0.35 mmol, Auer-Remy, 99.9%) and CsCl (1000 mg/6 mmol, Chempur, 99.99%); *Ln* = Nd: mixture of Nd (160 mg/1.11 mmol, Chempur, 99.99%), $NdCl_3$

(200 mg/0.80 mmol, Chempur, 99.9%), Nd_2O_3 (80 mg/0.24 mmol) and CsCl (1000 mg/6 mmol, Chempur, 99.99%).

The reactions yielded comparatively large single crystals of globular (diameter up to 0.2 mm) and needle-like shape (length up to 3 mm) together with $Ln_3Si_6N_{11}$ [12–14] as a crystalline by-product. The desired crystals could be separated from the by-products due to their differing crystal habit and color.

2.2. Crystal-structure analysis

2.2.1. Single-crystal X-ray analysis

X-ray diffraction data of $Ln_4[Si_4O_{3+x}N_{7-x}]Cl_{1-x}O_x$ with Ln = Ce, Pr, Nd were collected on a four-circle diffractometer (Stoe Stadi4) using Mo$K\alpha$ radiation. The diffraction data were corrected for an intensity decay (Ce: 12.5%, Pr: 8.0%, Nd: 5.1%). According to the observed reflection conditions ($0\,0\,l$ with $l = 2n$) of the cubic lattice, the space group $P2_13$ (no. 198) was determined. The crystal structure of $Ln_4[Si_4O_{3+x}N_{7-x}]Cl_{1-x}O_x$ was solved by direct methods using SHELXTL [15] and refined with anisotropic thermal displacement parameters for all atoms (except for the split position Ce2). The site occupancy factors of the mixed O/N positions in the anionic layer were refined using constraints that guarantee the charge neutrality of the structure, depending on the *s.o.f.* of chlorine on the mixed O/Cl site (inside the complex cation). Relevant crystallographic data and details of the X-ray data collection are shown in Table 1. Table 2 gives the positional and thermal displacement parameters for all atoms. Table 3 lists selected interatomic distances and angles.

Details of the single-crystal structures of $Ln_4[Si_4O_{3+x}N_{7-x}]Cl_{1-x}O_x$ with Ln = Ce, Pr, Nd may be obtained from the Fachinformationszentrum Karlsruhe, D-76344 Eggenstein-Leopoldshafen, Germany, E-mail: crysdata@FIZ-karlsruhe.de, by quoting the depository numbers CSD-414399, CSD-414400 and CSD-414401.

2.2.2. Neutron powder diffraction

Time-of-flight (TOF) powder neutron diffraction measurements were conducted with a pure sample consisting of 520 mg of $Pr_4[Si_4O_{3+x}N_{7-x}]Cl_{1-x}O_x$ (ground single crystals), using the GEM diffractometer at ISIS/Rutherford Appleton Laboratory, Chilton/UK. During the diffraction experiment, which was performed at ambient temperature, the sample was enclosed in a vanadium cylinder. From the resulting six data banks, five banks (2θ: 18.0°, 35.0°, 63.6°, 91.3°, 154.4°) were used for a multi-bank Rietveld refinement (using the program GSAS [16]) owing to their relevant range of d-spacings from $d = 0.53-6.74$ Å (TOF 4.0–18.0 ms). The intensities were normalized against monitor intensities. For the refinement a starting model based on the X-ray single-crystal data of $Pr_4[Si_4O_{3+x}N_{7-x}]Cl_{1-x}O_x$

Table 1
Crystallographic data and details of the single-crystal X-ray data collection for $Ln_4[Si_4O_{3+x}N_{7-x}]Cl_{1-x}O_x$ with Ln = Ce, Pr, Nd

Rare-earth element, substitution factor	Ce, $x = 0.07$	Pr, $x = 0.31$	Nd, $x = 0.04$
Diffractometer, monochromator		Stoe STADI 4, graphite	
Radiation		Mo$K\alpha$ ($\lambda = 0.71073$ Å)	
Temperature (K)		293(2)	
Space group		$P2_13$ (No. 198), cubic	
Lattice parameter, a (Å)	10.4461(12)	10.3720(12)	10.3618(12)
Cell volume, V (Å^3)	1139.9(2)	1115.8(2)	1112.5(2)
Formula units		$Z = 4$	
Crystal size (mm^3)	0.130 × 0.125 × 0.116	0.115 × 0.057 × 0.050	0.115 × 0.107 × 0.103
Crystal color	Orange	Pale green	Pale violet
Calculated density (g/cm^3)	4.971	5.072	5.194
Diffraction range (°)	$3<2\theta<70$	$3<2\theta<70$	$3<2\theta<70$
Measured reflections	7558	5516	4589
Independent reflections	1679	1645	1641
Observed reflections	1449	1513	1588
Ref. parameters/restraints	66/3	67/3	67/3
R_{int}	0.0962	0.0481	0.0261
$F(000)$	1510	1518	1542.6
Extinction coefficient, χ	0.0029(2)	0.00091(9)	0.00155(7)
Absorption correction		Semi-empirical, psi-scans	
Absorption coefficient (mm^{-1})	16.320	17.765	19.028
Min./max. transmission	0.120/0.151	0.355/0.411	0.141/0.103
Flack parameter	−0.06(4)	−0.01(3)	0.00(2)
Min./max. residual electron density (e/Å^3)	−1.626/1.833	−2.347/2.531	−1.342/2.656
GooF	1.101	1.146	1.102
$R_1[I>2\sigma(I)]$	0.0524[0.0365]	0.0415[0.0340]	0.0257[0.0242]
w$R_2[I>2\sigma(I)]$	0.0746[0.0682]	0.0621[0.0596]	0.0517[0.0512]

Table 2
Atomic coordinates and anisotropic displacement parameters (Å^2) for $Ln_4[Si_4O_{3+x}N_{7-x}]Cl_{1-x}O_x$ with Ln = Ce, Pr, Nd determined by single-crystal X-ray diffraction with e.s.d.s in parentheses

Atom	Wyck	*x*	*y*	*z*	*s.o.f.*	U_{eq}	U_{11}	U_{22}	U_{33}	U_{23}	U_{13}	U_{12}
Ce1	12*b*	−0.81503(4)	−0.69243(4)	−0.04433(4)	1	0.00887(11)	0.00896(19)	0.01008(19)	0.00756(19)	−0.00157(14)	0.00081(14)	−0.00005(15)
Ce2	4*a*	−0.0375(18)	x	x	0.035(4)	0.026(7)						
Ce3	4*a*	−0.10470(4)	x	x	0.965(4)	0.00946(18)	0.00946(18)	U_{11}	U_{11}	0.00054(15)	U_{23}	U_{23}
Si1	12*b*	−0.07913(18)	−0.74540(19)	−0.1963(2)	1	0.0057(3)	0.0044(7)	0.0065(8)	0.0062(7)	−0.0014(7)	−0.0001(7)	−0.0001(6)
Si2	4*a*	−0.42787(19)	x	x	1	0.0052(6)	0.0052(6)	U_{11}	U_{11}	0.0007(6)	U_{23}	U_{23}
O1	4*a*	−0.3360(5)	x	x	1	0.0116(18)	0.0116(18)	U_{11}	U_{11}	−0.0011(19)	U_{23}	U_{23}
Cl	4*a*	−0.9274(2)	x	x	0.928(10)	0.0137(7)	0.0137(7)	U_{11}	U_{11}	0.0008(7)	U_{23}	U_{23}
O2					0.072(10)							
O3	12*b*	−0.9286(5)	−0.7884(5)	−0.2364(6)	0.690(4)	0.0086(10)	0.007(2)	0.007(2)	0.012(2)	−0.0029(19)	−0.0001(18)	0.0014(17)
N3a					0.310(4)							
N1	12*b*	−0.1290(6)	−0.6519(6)	−0.3244(6)	1	0.0084(11)	0.007(3)	0.012(3)	0.006(2)	0.002(2)	−0.001(2)	−0.005(2)
N2	12*b*	−0.0585(7)	−0.6357(6)	−0.0766(6)	1	0.0126(13)	0.017(3)	0.009(3)	0.012(3)	−0.006(2)	−0.004(2)	0.002(2)
Pr1	12*b*	−0.81623(4)	−0.69734(4)	−0.04081(4)	1	0.01317(9)	0.00912(16)	0.01856(19)	0.01182(17)	−0.00760(14)	0.00064(12)	0.00039(13)
Pr2	4*a*	−0.03181(16)	x	x	0.246(3)	0.0149(7)	0.0149(7)	U_{11}	U_{11}	−0.0014(6)	U_{23}	U_{23}
Pr3	4*a*	−0.10631(5)	x	x	0.754(3)	0.01076(19)	0.01076(19)	U_{11}	U_{11}	0.00152(16)	U_{23}	U_{23}
Si1	12*b*	−0.07718(16)	−0.74803(16)	−0.19673(18)	1	0.0062(3)	0.0056(6)	0.0078(7)	0.0052(6)	0.0004(6)	−0.0003(5)	−0.0008(5)
Si2	4*a*	−0.42776(17)	x	x	1	0.0066(5)	0.0066(5)	U_{11}	U_{11}	0.0011(6)	U_{23}	U_{23}
O1	4*a*	−0.3353(5)	x	x	1	0.0114(15)	0.0114(15)	U_{11}	U_{11}	−0.0024(15)	U_{23}	U_{23}
Cl	4*a*	−0.9257(2)	x	x	0.693(10)	0.0171(8)	0.0171(8)	U_{11}	U_{11}	0.0044(8)	U_{23}	U_{23}
O2					0.307(10)							
O3	12*b*	−0.9278(5)	−0.7948(6)	−0.2318(6)	0.769(4)	0.0195(12)	0.010(2)	0.029(3)	0.019(3)	−0.019(2)	−0.0014(18)	0.002(2)
N3a					0.231(4)							
N1	12*b*	−0.1267(6)	−0.6528(5)	−0.3255(6)	1	0.0119(10)	0.016(3)	0.009(2)	0.011(2)	0.0000(18)	−0.003(2)	−0.0040(19)
N2	12*b*	−0.0576(6)	−0.6370(6)	−0.0756(6)	1	0.0128(11)	0.018(3)	0.012(2)	0.011(2)	−0.0046(19)	−0.004(2)	0.003(2)
Nd1	12*b*	0.81585(3)	0.69352(3)	0.04398(3)	1	0.00971(7)	0.00865(11)	0.01171(12)	0.00877(11)	−0.00272(9)	0.00083(8)	0.00021(9)
Nd2	4*a*	0.0321(4)	x	x	0.071(3)	0.0167(19)	0.0167(19)	U_{11}	U_{11}	−0.0059(13)	U_{23}	U_{23}
Nd3	4*a*	0.10539(3)	x	x	0.929(3)	0.0103(2)	0.01034(12)	U_{11}	U_{11}	0.00172(10)	U_{23}	U_{23}
Si1	12*b*	0.07784(12)	0.74595(12)	0.19680(13)	1	0.0053(2)	0.0042(5)	0.0062(5)	0.0053(5)	0.0005(4)	0.0000(4)	−0.0009(4)
Si2	4*a*	0.42871(13)	x	x	1	0.0057(4)	0.0057(4)	U_{11}	U_{11}	0.0000(4)	U_{23}	U_{23}
O1	4*a*	0.3365(4)	x	x	1	0.0096(11)	0.0096(11)	U_{11}	U_{11}	−0.0005(11)	U_{23}	U_{23}
Cl	4*a*	0.92482(14)	x	x	0.956(10)	0.0153(5)	0.0153(5)	U_{11}	U_{11}	0.0013(4)	U_{23}	U_{23}
O2					0.044(10)							
O3	12*b*	0.9274(4)	0.7899(4)	0.2367(4)	0.681(4)	0.0105(7)	0.0057(14)	0.0134(16)	0.0124(16)	−0.0065(13)	0.0005(12)	0.0021(12)
N3a					0.319(4)							
N1	12*b*	0.1280(4)	0.6509(4)	0.3251(4)	1	0.0095(7)	0.0119(18)	0.0077(15)	0.0089(17)	0.0022(13)	−0.0004(13)	−0.0005(13)
N2	12*b*	0.0551(5)	0.6342(4)	0.0787(4)	1	0.0108(7)	0.0169(19)	0.0094(17)	0.0062(15)	−0.0035(12)	0.0001(14)	0.0020(15)

Labeling of the atoms according to Ref. [3]. U_{eq} is defined as one-third of the trace of the U_{ij} tensor. The anisotropic displacement factor exponent is of the form $-2\pi^2[(ha*)^2U_{11} + \cdots + 2hka*b*U_{12}]$. For Ce2 the anisotropic displacement factors could not be determined.

Table 3
Selected interatomic distances (Å) and angles (°) in the structure of $Ln_4[Si_4O_{3+x}N_{7-x}]Cl_{1-x}O_x$ with Ln = Ce, Pr, Nd determined by single-crystal X-ray diffraction with standard deviations in parentheses

Ce1–Ce2	3.861(19)[a] 4.289(19)[b]	Pr1–Pr2	3.862(2)[a] 4.128(2)[b]	Nd1–Nd2	3.8381(6)[a] 4.165(4)[b]
Ce1–Ce1	3.945(1)[a] 4.571(1)[b]	Pr1–Pr1	3.944(1)[a] 4.431(1)[b]	Nd1–Nd1	3.917(1)[a] 4.515(1)[b]
Ce2–Ce3	1.22(3)	Pr2–Pr3	1.338(3)	Nd2–Nd3	1.316(7)
Ce1–Ce3	4.109(1)[a] 5.301(1)[b]	Pr1–Pr3	4.122(1)[a] 5.245(1)[b]	Nd1–Nd3	4.092(1)[a] 5.255(1)[b]
Ce1–O/Cl	2.9823(18)	Pr1–O/Cl	2.885(2)	Nd1–O/Cl	2.9230(12)
Ce2–O/Cl	1.99(3)	Pr2–O/Cl	1.906(5)	Nd2–O/Cl	1.925(7)
Ce3–O/Cl	3.208(4)	Pr3–O/Cl	3.245(4)	Nd3–O/Cl	3.241(3)
Si1–N1	1.718(6)	Si1–N1	1.707(6)	Si1–N1	1.715(5)
Si1–N1	1.738(7)	Si1–N1	1.739(6)	Si1–N1	1.734(4)
Si1–N2	1.709(7)	Si1–N2	1.716(6)	Si1–N2	1.701(4)
Si1–O3/N3a	1.689(6)	Si1–O3/N3a	1.664(6)	Si1–O3/N3a	1.675(4)
Si2–O1	1.662(10)	Si2–O1	1.662(9)	Si2–O1	1.655(7)
Si2–N2 (3 ×)	1.696(7)	Si2–N2 (3 ×)	1.681(6)	Si2–N2 (3 ×)	1.694(4)
Si1–N1–Si1	122.0(4)	Si1–N1–Si1	121.8(3)	Si1–N1–Si1	121.4(3)
Si1–N2–Si2	157.2(5)	Si1–N2–Si2	157.7(4)	Si1–N2–Si2	155.3(3)

[a]Shortest distance between [(O/Cl)Ln_4]-tetrahedra.
[b]Intra-tetrahedral distance.

Table 4
Crystallographic data and details of the neutron diffraction data collection and the Rietveld refinement for $Pr_4[Si_4O_{3+x}N_{7-x}]Cl_{1-x}O_x$

Diffractometer	GEM, ISIS
Temperature (K)	293(2)
Lattice parameter, a (Å)	10.37901(8)
Cell volume, V (Å^3)	1118.067(14)
Calculated density (g/cm^3)	5.076
Detector positions 2θ (°)	17.98, 4.96, 63.62, 91.30, 154.40
Scan mode	TOF
Number of Bragg reflections (banks 2–6)	15, 42, 218, 521, 1269
Observed reflections (total)	2065
Ref. Parameters	142
GooF (all data)	2.65
R_{wp} (banks 2–6)	0.0242, 0.0255, 0.0212, 0.0177, 0.0198
R_{F^2} (banks 2–6)	0.0131, 0.0245, 0.0343, 0.0309, 0.0355
Red. χ^2	7.012

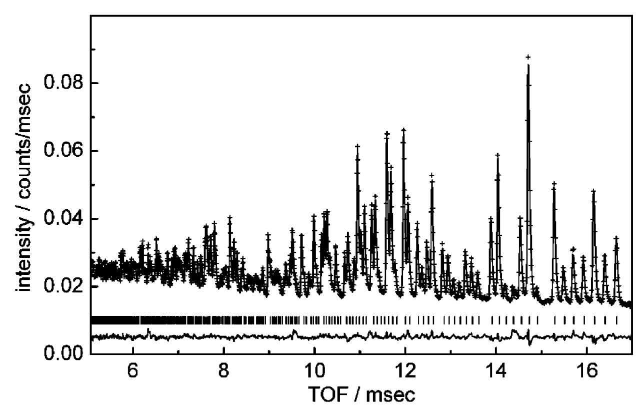

Fig. 2. Rietveld profile fit of the backscattering data (bank 6, 5–17 ms, $d = 0.53-1.88$ Å, $2\theta = 154.4°$) at ambient temperature. Observed (crosses) and calculated (line) neutron powder diffractograms as well as difference profile (lower line). The row of vertical lines indicates the possible reflection positions of $Pr_4[Si_4O_{3+x}N_{7-x}]Cl_{1-x}O_x$.

was used. Initially, O and N were located equally on the same crystallographic anion positions and their occupancy factors were refined dependently to sum up to 1. A free refinement of all O and N site occupancy factors lead to $s.o.f. = 0.998(7)$ for nitrogen on the N2/O2a site (labeling according to Ref. [3]), which was therefore fixed to 1. The thermal displacement parameters of Si1 and Si2 went negative during the refinement procedure, which is not unusual for a poorly scattering atom, Si, in the presence of strongly scattering partially absorbing atoms, Pr. Therefore, they were fixed to a reasonable value of 0.0015. Relevant crystallographic data and details of the neutron diffraction data collection and the Rietveld refinement are shown in Table 4. The results of the refinement of the backscattering data are illustrated exemplarily in Fig. 2, the positional and thermal displacement parameters and the occupancy factors for all atoms resulting from the multibank refinement (bank 2–6) are summarized in Table 5.

Details of the structure refinement from powder neutron diffraction data of $Pr_4[Si_4O_{3+x}N_{7-x}]Cl_{1-x}O_x$ may be obtained from the Fachinformationszentrum Karlsruhe, D-76344 Eggenstein-Leopoldshafen, Germany, E-mail: crysdata@FIZ-karlsruhe.de, by quoting the depository number CSD-414402.

Table 5
Positional coordinates and displacement factors (Å, e.s.d.s in parentheses) resulting from the Rietveld multibank refinement of the powder neutron diffraction of $Pr_4[Si_4O_{3+x}N_{7-x}]Cl_{1-x}O_x$ at ambient temperature

Atom	Wyck	x	y	z	U_{iso}	*s.o.f.*
Pr1	12*b*	0.81507(16)	0.69399(14)	0.04351(15)	0.0048(4)	1
Pr2	4*a*	0.037(2)	—	—	0.0048(4)	0.116(5)
Pr3	4*a*	0.10595(18)	—	—	0.0048(4)	0.884(5)
Si1	12*b*	0.07872(18)	0.74610(15)	0.19591(14)	0.0015[a]	1
Si2	4*a*	0.42728(15)	—	—	0.0015[a]	1
O1	4*a*	0.33591(10)	—	—	0.0041(8)	0.929(11)
N1a						0.071(11)
Cl	4*a*	0.92544(8)	0.92544(8)	0.92544(8)	0.0097(5)	0.792(7)
O2						0.208(7)
O3	12*b*	0.92767(11)	0.78900(10)	0.23610(10)	0.0077(4)	0.705(7)
N3a						0.295(7)
N1	12*b*	0.12773(6)	0.65231(7)	0.32540(6)	0.0019(3)	0.941(8)
O1a						0.059(8)
N2	12*b*	0.05701(8)	0.63547(8)	0.07774(8)	0.0064(3)	1

[a]The isotropic displacement factors could not be determined and were fixed to a reasonable value.

2.2.3. X-ray powder diffraction

Powder diffraction patterns were obtained from single-phase samples of $Ln_4[Si_4O_{3+x}N_{7-x}]Cl_{1-x}O_x$ with Ln = Ce, Pr, Nd using a Stoe Stadi P diffractometer in Debye–Scherrer geometry. The compounds were measured in glass capillaries (Hilgenberg, $\varnothing = 0.2$ mm). All of the detected reflections, except three very weak ones, have been indexed and Rietveld refinements were performed (using GSAS). A structural model with a fully occupied Cl-site and defined fixed occupancies of the O, N and O/N positions was employed and some of the isotropic thermal displacement parameters had to be fixed to reasonable values in order to perform a stable refinement. Relevant crystallographic data and details of the powder X-ray data collection are shown in Table 6. The refined powder patterns are shown in Fig. 3. The atom positions, isotropic thermal displacement parameters and occupancy factors are listed in Table 7.

Table 6
Crystallographic data and details of the powder X–ray data collection for $Ln_4[Si_4O_{3+x}N_{7-x}]Cl_{1-x}O_x$ with Ln = Ce, Pr, Nd

Rare-earth element	Ce	Pr	Nd
Diffractometer		Stoe Stadi P	
Monochromator		Germanium	
Radiation		Mo$K\alpha$ ($\lambda = 0.7093$ Å)	
Temperature (K)		293(2)	
Sample container		Glass capillary	
Background		Fixed	
Lattice parameter, a (Å)	10.42939(7)	10.38570(6)	10.35226(6)
Cell volume, V/Å^3	1134.427(14)	1120.230(11)	1109.444(11)
Calculated density (g/cm^3)	5.002	5.084	5.213
Diffraction range (°)	$3<2\theta<65$	$3<2\theta<65$	$3<2\theta<65$
Observed reflections	787	777	771
Ref. Parameters	38	28	31
GooF	0.94	0.96	1.17
R_{F^2}	0.0387	0.0538	0.0547
wR_p	0.0362	0.0450	0.0457
Red. χ^2	0.8804	0.9201	1.376

2.3. Magnetic measurements

The magnetic susceptibilities of polycrystalline, powdered samples of $Ce_4[Si_4O_{3.2}N_{6.8}]Cl_{0.8}O_{0.2}$ (31.90 mg) and $Pr_4[Si_4O_{3.2}N_{6.8}]Cl_{0.8}O_{0.2}$ (22.30 mg) (chemical composition fixed at $x = 0.2$ for the calculations; changes of ± 0.1 showed very little influence) were determined with a MPMS SQUID magnetometer (Quantum Design, Inc.) in a temperature range from 2 to 300 K with magnetic flux densities up to 5.5 T. The samples were cooled to 2 K in zero magnetic field and slowly heated to room temperature in the applied external fields.

2.4. Vibrational spectroscopy

FTIR spectra (Fig. 4) were measured at room temperature by using a Bruker IFS 66v/S spectrometer. The samples were thoroughly ground together with dried KBr (1 mg sample/250 mg KBr) in a glove box under argon atmosphere.

2.5. Chemical analysis and EPMA

The chemical analysis (precision: $\approx 0.5\%$(O, N, Si, Cl), $\approx 1.0\%$(Pr)) of $Pr_4[Si_4O_{3+x}N_{7-x}]Cl_{1-x}O_x$ was executed by Mikroanalytisches Labor Pascher,

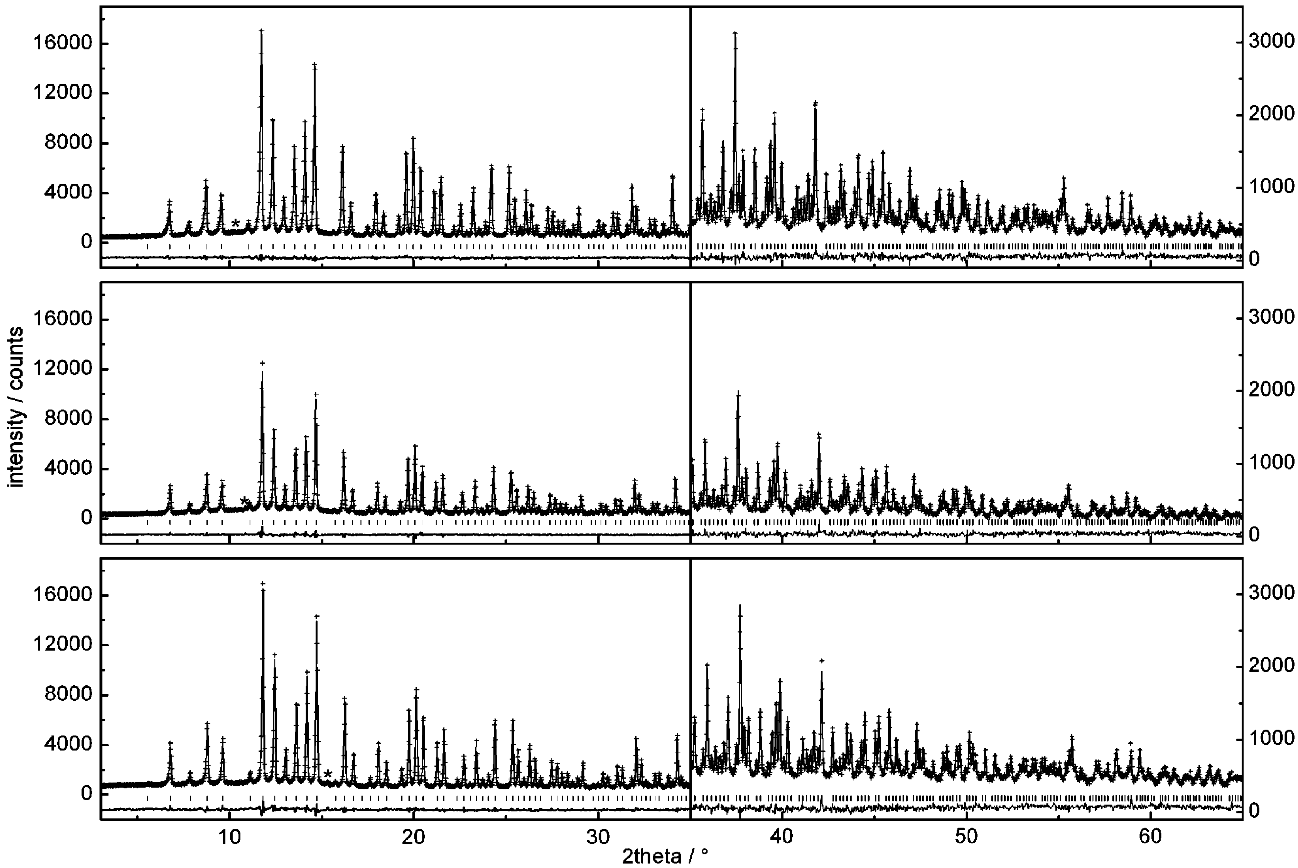

Fig. 3. Rietveld profile fits of the X-ray powder diffraction data of $Ln_4[Si_4O_{3+x}N_{7-x}]Cl_{1-x}O_x$ with Ln = Ce, Pr, Nd (Mo$K\alpha$ = 0.71730 Å, 2θ = 3–65°). Observed (crosses) and calculated (line) diffractograms as well as the difference profile (lower line). The row of vertical lines indicates the possible reflection positions. Not indexed reflections are marked by an asterisk. Top: $Ce_4[Si_4O_{3+x}N_{7-x}]Cl_{1-x}O_x$, middle: $Pr_4[Si_4O_{3+x}N_{7-x}]Cl_{1-x}O_x$, and bottom: $Nd_4[Si_4O_{3+x}N_{7-x}]Cl_{1-x}O_x$.

Remagen. Each element of the sample (30 mg) was analyzed twice, the results are listed in Table 8.

Quantitative chemical analyses on the microscale by electron probe microanalysis (EPMA) were carried out with the Jeol JXA-8900R superprobe using an accelerating voltage of 15 kV, a beam current of 80 nA and a 3 μm measuring spot. The total volume analyzed is around 10–15 μm^3. The microprobe is equipped with synthetic multilayer spectrometer crystals with large d-spacing for quantitative wavelength dispersive analysis of light elements. For N and O analysis, the LDE1 crystal with $2d = 600$ nm was used. Matrix correction was carried out with the CITZAF program [17]. For microprobe analysis, the samples were mounted with epoxy resin into cylindrical holes in an epoxy pellet of 25 mm diameter and polished with a final diamond powder grain size of 0.25 μm.

Since the quantitative analysis of light elements such as N and O, and also of Cl, are not a routine EPMA technique (see Refs. [18,19]), great care was taken to minimize errors that may occur during measurements of these low-energy X-ray emission lines. In addition, the analysis of light elements becomes more difficult in the presence of the various rare-earth elements in high concentrations in the oxonitridosilicate chlorides. They produce a large number of emission lines which may overlap with the N, O or Cl$K\alpha$ lines. Thus, the following precautions and measuring procedures were chosen.

(i) To prevent surface oxidation and absorption effects by the carbon coating, the samples were polished shortly before the measurements, cleaned in p.a. petrolether in an ultrasonic cleaner and vacuum dried. The samples and the N standard were coated with carbon under high-vacuum conditions simultaneously to ensure an identical carbon coat thickness for all of the samples. The carbon layer thickness of about 15 nm was controlled by interference colors on a polished brass surface.

(ii) The peak shape was monitored by wavelength dispersive scans over the measuring regions of all of the peaks of the elements to be analyzed. Hence it could be shown that there is no peak shape difference of the light element $K\alpha$ emission between standards and samples. It was therefore possible to use peak intensity measurements at the peak

Table 7
Positional coordinates and displacement factors (Å, e.s.d.s in parentheses) resulting from the Rietveld refinements of the X-ray powder data of $Ln_4[Si_4O_{3+x}N_{7-x}]Cl_{1-x}O_x$ with *Ln* = Ce, Pr, Nd at ambient temperature

Atom	Wyck	*x*	*y*	*z*	U_{iso}	*s.o.f.*
Ce1	12*b*	0.81552(7)	0.69394(6)	0.04368(5)	0.01289(7)	1
Ce2	4*a*	0.038(1)	x	x	0.01289(7)	0.066(2)
Ce3	4*a*	0.10490(7)	x	x	0.01289(7)	0.934(2)
Si1	12*b*	0.0780(3)	0.7452(2)	0.1982(3)	0.0143(8)	1
Si2	4*a*	0.4282(4)	x	x	0.0150(13)	1
O1	4*a*	0.3304(7)	x	x	0.0150[a]	1
Cl	4*a*	0.9275(3)	x	x	0.0247(13)	1
O3	12*b*	0.9273(6)	0.7915(6)	0.2347(5)	0.0074(19)	2/3
N3a						1/3
N1	12*b*	0.1255(6)	0.6511(5)	0.3204(6)	0.0031(18)	1
N2	12*b*	0.0611(7)	0.6362(7)	0.0779(7)	0.009(2)	1
Pr1	12*b*	0.81582(9)	0.69450(9)	0.04359(7)	0.01139(8)	1
Pr2	4*a*	0.034(1)	x	x	0.01139(8)	0.086(2)
Pr3	4*a*	0.10492(9)	x	x	0.01139(8)	0.914(2)
Si1	12*b*	0.0768(4)	0.7447(4)	0.1984(4)	0.0151(9)	1
Si2	4*a*	0.4274(4)	x	x	0.0151(9)	1
O1	4*a*	0.3304(9)	x	x	0.0150[a]	1
Cl	4*a*	0.9266(4)	x	x	0.0209(16)	1
O3	12*b*	0.9275(8)	0.7881(9)	0.2353(8)	0.0150[a]	2/3
N3a						1/3
N1	12*b*	0.1232(9)	0.6484(8)	0.3237(10)	0.0150[a]	1
N2	12*b*	0.0562(10)	0.6340(10)	0.0822(10)	0.013(4)	1
Nd1	12*b*	0.81620(9)	0.69347(9)	0.04443(8)	0.01278(8)	1
Nd2	4*a*	0.029(2)	x	x	0.01278(8)	0.063(2)
Nd3	4*a*	0.10512(9)	x	x	0.01278(8)	0.937(2)
Si1	12*b*	0.0778(4)	0.7467(4)	0.1978(5)	0.0161(12)	1
Si2	4*a*	0.4291(5)	x	x	0.0203(21)	1
O1	4*a*	0.3335(9)	x	x	0.0150[a]	1
Cl	4*a*	0.9260(4)	x	x	0.027(3)	1
O3	12*b*	0.9281(8)	0.7878(9)	0.2376(8)	0.010(3)	2/3
N3a						1/3
N1	12*b*	0.1269(8)	0.6495(7)	0.3277(9)	0.002(3)	1
N2	12*b*	0.0530(11)	0.6342(10)	0.0824(10)	0.012(4)	1

[a]The isotropic displacement factors could not be determined and were fixed to a reasonable value.

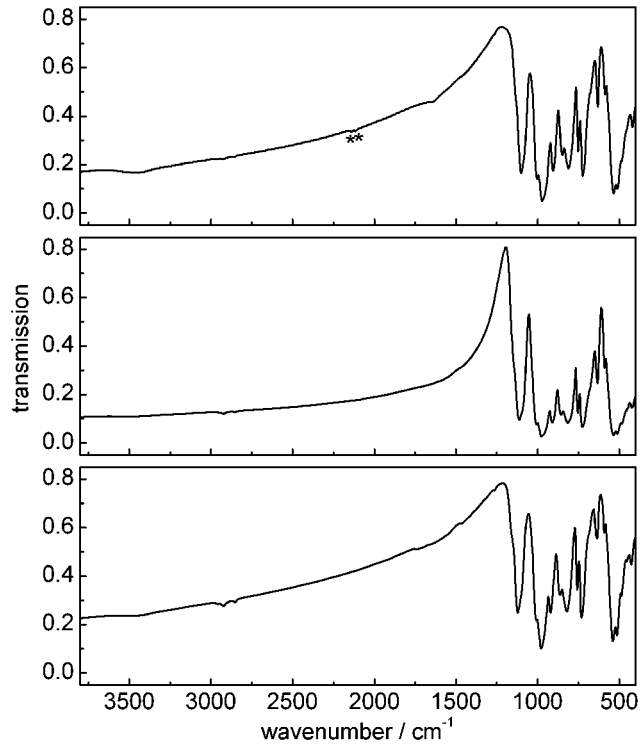

Fig. 4. FTIR spectra of $Ln_4[Si_4O_{3+x}N_{7-x}]Cl_{1-x}O_x$ with *Ln* = Ce (top), Pr (middle), Nd (bottom) recorded at ambient temperature. Asterisks mark assumed electronic transitions, characteristic for the cerium compound. The peaks around 2900 cm^{-1} derive from the preparation ($-CH_3$).

Table 8
Results of the chemical analyses (all values given in wt%) of $Pr_4[Si_4O_{3+x}N_{7-x}]Cl_{1-x}O_x$

	Pr	Si	O	N	Cl	Total
Measured	64.3/	13.1/	7.94/	12.0/	3.24/	
	64.1	13.2	7.55	12.0	3.32	
Average	64.2	13.15	7.75	12.0	3.28	100.4
Calculated for $x = 0.2$	66.0	13.2	6.37	11.1	3.33	100.0

maximum for the light elements. In addition, the spectra were used to define the peak and background measuring positions for the light elements taking into account the overlaps by rare-earth elements.

(iii) For the quantification of light element X-ray emission, the choice of appropriate standards is crucial. Chemical composition and crystallographic structure of standards and samples should be chosen to be as similar as possible. We therefore used stoichiometric crystals of $Ce_3Si_6N_{11}$ [14] as standards for N, as well as for Ce and Si. The silicate mineral albite was chosen as an oxygen standard (no. 131705 [20]) since albite is a framework silicate and therefore comes structurally close to the oxonitridosilicate chlorides. For the standardization of Cl, the mineral standard scapolite was used (USNM R6600-1 [21]) and $NdPO_4$ for Nd (USNM 168492 [22]). Details of measuring conditions, standards and detection limits are given in Table 9. Detection limits were calculated from oxonitridosilicate chlorides which contain 20.7 wt% N, 6.3 wt% O and 3.6 wt% Cl. They are 870, 320 and 17 ppm, respectively.

2.6. X-ray absorption spectroscopy (XAS)

The Ce-L_{III} XAS spectrum of polycrystalline $Ce_4[Si_4O_{3+x}N_{7-x}]Cl_{1-x}O_x$ was recorded in transmission

Table 9
Parameters of the EPMA measurements

Element, X-ray line	Standard	Spectrometer crystal	Measuring time on peak (s)	Measuring time on background (s)
Ce, Lα	$Ce_3Si_6N_{11}$ [14]	PET	90	45 + 45
Pr, Lα	$Pr_3Si_6N_{11}$ [12]	PET	60	30 + 30
Nd, Lα	$NdPO_4$ [22]	PET	60	30 + 30
Si, Kα	$Ce_3Si_6N_{11}$	TAP	90	90
N, Kα	$Ce_3Si_6N_{11}$	LDE1	120	60 + 60
O, Kα	Albite [20]	LDE1	40	20 + 20
Cl, Kα	Scapolite [21]	PETH	180	90 + 90

geometry at the EXAFS-II beamline of HASYLAB/DESY laboratories (Hamburg, Germany) using a Si(111) double-crystal monochromator. This resulted in an experimental resolution of 1.5 eV (FWHM) at the Ce-L_{III} threshold (5.72 keV). Homogeneous absorbers were prepared by grinding the studied material together with dry B_4C powder. The absorption spectrum was measured simultaneously with the spectrum of CeO_2, the latter serving as a reference for energy calibration.

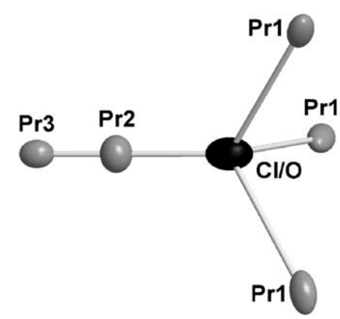

Fig. 5. The complex cation $[Cl_{1-x}O_xPr_4]^{(11-x)+}$ exhibiting the Pr2/Pr3 split position. Displacement ellipsoids are drawn at the 90% probability level. Pr: gray ellipsoids, Cl/O: black ellipsoid.

3. Results and discussion

3.1. Crystal structure

The partial substitution of oxygen with chlorine in the complex cations $[OCe_4]^{10+}$ of $Ce_4[Si_4O_4N_6]O$ results in $[Cl_{1-x}O_xLn_4]^{(11-x)+}$ (Fig. 5). To restore the charge balance a lack of Ln^{3+} may be assumed, but no reduced *s.o.f.*'s for the lanthanides could be found. Therefore, the anionic network $[Si_4O_4N_6]^{10-}$ was expected to change to $[Si_4O_{3+x}N_{7-x}]^{(11-x)-}$, containing more N^{3-}, thereby compensating for the deficiency of negative charge.

In order to proof the existence of a $[Si_4O_{3+x}N_{7-x}]^{(11-x)-}$ network, we performed powder neutron diffraction measurements. Thereby an unequivocal experimental discrimination of N and O is possible, due to the significant difference of their neutron scattering lengths ($b(N) = 9.36 \times 10^{-15}$ m, $b(O) = 5.80 \times 10^{-15}$ m). For the extra nitrogen two different crystallographic sites (O1, O3), which were originally fully occupied by oxygen, have been taken into account. The neutron diffraction data showed that in $Pr_4[Si_4O_{3+x}N_{7-x}]Cl_{1-x}O_x$ a mixing of O and N occurs mainly at one crystallographic site (O3/N3a, Wyck.-position 12*b*). This terminal site is bound to the 3-ring unit made up of $SiON_3$ tetrahedra of $Ce_4[Si_4O_4N_6]O$. Thus, the measurements revealed the crystallographic position of the incorporated nitrogen (Fig. 6).

The *Ln*2/*Ln*3 split position observed in $Ce_4[Si_4O_4N_6]O$ can also be detected in $Ln_4[Si_4O_{3+x}N_{7-x}]Cl_{1-x}O_x$ with *Ln* = Ce, Pr, Nd. The site occupancy factors differ strongly, they switch from 5:1 ($Ce_4[Si_4O_4N_6]O$) to around 1:10 ($Ln_4[Si_4O_{3+x}N_{7-x}]Cl_{1-x}O_x$). This might be caused by the larger chlorine atom substituting the smaller oxygen atom. A correlation concerning the degree of chlorine incorporation and the occupancy of the *Ln*3 site can be observed within 1.5 e.s.d.'s from single-crystal X-ray diffraction data.

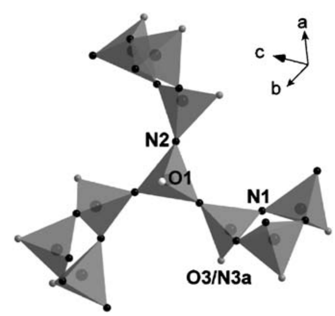

Fig. 6. Fragment of the anionic network $[Si_4O_4N_6]^{10-}$ of $Ce_4[Si_4O_4N_6]O$ showing the four crystallographically different positions for O or N. Silicon atoms are shown inside the tetrahedra, terminal O (O1, part of connecting tetrahedron): white circle, terminal O (O3/N3a, part of dreier-ring-tetrahedra): gray circles, connecting N (N1, N2): black circles. Labeling according to Ref. [3].

Furthermore, the site occupancy factor of the O/Cl position for $Pr_4[Si_4O_{3+x}N_{7-x}]Cl_{1-x}O_x$ has been determined by four different methods and the results could be compared to each other (neutron powder diffraction: 0.792(7), single-crystal X-ray diffraction: 0.69(2), chemical analysis: 0.79(2), EPMA: 0.86(3)). The X-ray powder diffraction method was not sensitive enough to extract the O/Cl occupancy.

The absence of hydrogen (N–H) was established by IR spectroscopy (Fig. 4). Furthermore, two characteristic peaks at about 2110 and 2140 cm^{-1} were observed in the spectrum of the cerium compound and assumed to represent electronic transitions. The peaks have been object of pressure-dependent IR spectroscopy. The results will be published in a forthcoming paper.

3.2. Magnetic properties

The temperature dependence of the inverse magnetic susceptibility of $Ce_4[Si_4O_{3.2}N_{6.8}]Cl_{0.8}O_{0.2}$ and $Pr_4[Si_4O_{3.2}N_{6.8}]Cl_{0.8}O_{0.2}$ (chemical composition fixed at $x = 0.2$ for the calculations) is displayed in Figs. 7 and 8. The high-temperature parts of the $1/\chi$ vs. T plots (data above 100 K) are almost linear. An evaluation of the data for the cerium compound according to a modified Curie–Weiss expression $\chi = \chi_0 + C/(T - \Theta)$ resulted in an experimental magnetic moment of 2.15(5) μ_B per cerium atom, a temperature-independent contribution $\chi_0 = 2.0(1) \times 10^{-3}$ cm^3/mol, and a paramagnetic Curie temperature (Weiss constant) of $\Theta = -23(1)$ K. The experimental magnetic moment is slightly smaller than the μ_{eff} value of 2.54 μ_B expected for the free Ce^{3+} ion [23]. The $1/\chi$ plot shows significant deviations from Curie–Weiss behavior below 100 K, most likely due to crystal field splitting of the $J = 5/2$ ground state of Ce^{3+}. No magnetic ordering is evident down to 2 K. The magnetic behavior of $Ce_4[Si_4O_{3.2}N_{6.8}]Cl_{0.8}O_{0.2}$ is similar to that of $Ce_3Si_6N_{11}$ [14].

The $1/\chi$ plot of $Pr_4[Si_4O_{3.2}N_{6.8}]Cl_{0.8}O_{0.2}$ shows a much smaller curvature and the data above 14 K have been fitted to the Curie–Weiss law yielding $\mu_{exp} =$ 3.50(5) μ_B per praseodymium atom and $\Theta = -27(1)$ K. The μ_{exp} value is close to that of $\mu_{eff} = 3.58$ μ_B for the free Pr^{3+} ion ($J = 4$ ground state), indicating that the Pr 4f electrons are almost localized [23]. No magnetic ordering was observed down to 2 K. The influence of the crystal electric field is less pronounced in $Pr_4[Si_4O_{3.2}N_{6.8}]Cl_{0.8}O_{0.2}$ as compared to $Ce_4[Si_4O_{3.2}N_{6.8}]Cl_{0.8}O_{0.2}$.

The magnetization vs. external field data of the praseodymium compound at 2 and 50 K are displayed in Fig. 9. At 50 K, the magnetization shows a linear increase as expected for a paramagnetic material. A steeper increase of the magnetization is observed at 2 K with a magnetic moment of 1.82(5) μ_B/Pr atom at the highest obtainable field strength of 5.5 T, which is smaller than the maximal value of 3.20 μ_B/Pr atom according to $g \times J$ [23]. Such small magnetization values are also known from various intermetallic praseodymium compounds [24]. The magnetization data give no hint for a field-induced magnetic transition.

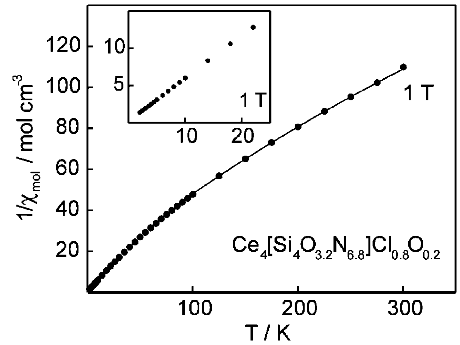

Fig. 7. Temperature dependence of the inverse magnetic susceptibility of $Ce_4[Si_4O_{3.2}N_{6.8}]Cl_{0.8}O_{0.2}$ measured at an external flux density of 1 T. The solid line corresponds to the Curie–Weiss fit discussed in the text. The low-temperature behavior is shown in the inset.

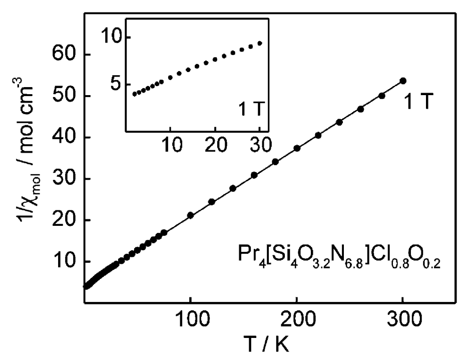

Fig. 8. Temperature dependence of the inverse magnetic susceptibility of $Pr_4[Si_4O_{3.2}N_{6.8}]Cl_{0.8}O_{0.2}$ measured at an external flux density of 1 T. The solid line corresponds to the Curie–Weiss fit discussed in the text. The low-temperature behavior is shown in the inset.

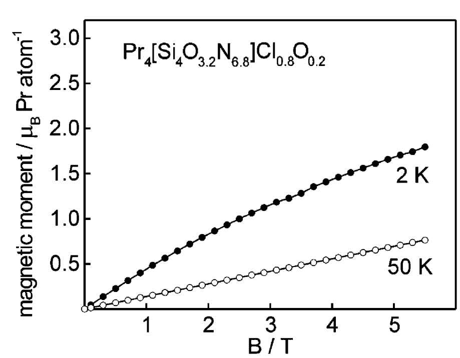

Fig. 9. Magnetization vs. external magnetic flux density of $Pr_4[Si_4O_{3.2}N_{6.8}]Cl_{0.8}O_{0.2}$ measured at 2 and 50 K.

3.3. X-ray absorption spectroscopy

For independent information on the electronic state of cerium, XAS spectra on the Ce-L_{III} threshold were

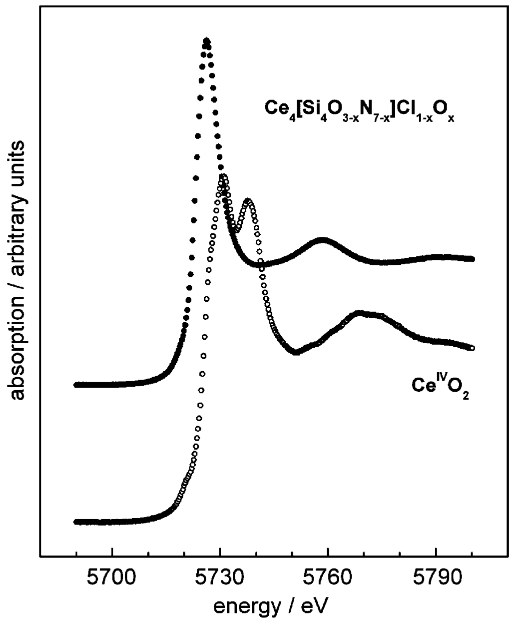

Fig. 10. XAS spectra at the Ln-L_{III} edge of $Ce_4[Si_4O_{3+x}N_{7-x}]Cl_{1-x}O_x$ (rings) and $Ce^{VI}O_2$ (crosses) for comparison.

measured. The applied range of photon energies made it possible to measure in transmission geometry, so that data of the bulk material less obscured by surface impurities could be obtained. Fig. 10 shows the Ce-L_{III} edge of $Ce_4[Si_4O_{3+x}N_{7-x}]Cl_{1-x}O_x$ together with the spectrum of $Ce^{IV}O_2$ as a reference.

Unlike Ce($4f^1$) compounds exhibiting a single peak structure in the Ln-L_{III} spectra, the Ln-L_{III} XAS spectrum of Ce($4f^0$) compounds exhibits two maxima. This is attributed to covalency effects based on a partial back-donation of charge from the formally closed shell anions [25]. The spectrum of $Ce_4[Si_4O_{3+x}N_{7-x}]Cl_{1-x}O_x$ displays one maximum; furthermore, the absorption maximum significantly differs from that of $Ce^{IV}O_2$ (Fig. 10). Both facts indicate a pure Ce($4f^1$) state in $Ce_4[Si_4O_{3+x}N_{7-x}]Cl_{1-x}O_x$.

3.4. Chemical analysis and EPMA

The elemental analysis (Mikroanalytisches Labor Pascher, Remagen, proclaimed precision ≈0.3% for O, N and Si, ≈0.2% for Cl, ≈1%for Pr) for $Pr_4[Si_4O_{3+x}N_{7-x}]Cl_{1-x}O_x$ (Table 8) agrees with the theoretical values for Pr and Si and gives differing values for N and O, which might occur due to difficulties during standardization. Taking into account the obtained values for the chlorine content of the substance, an approximated formula $Pr_4Si_4[O_{3.2}N_{6.8}]Cl_{0.8}O_{0.2}$ could be calculated.

Using EPMA, various crystals of $Ln_4[Si_4O_{3+x}N_{7-x}]Cl_{1-x}O_x$ with Ln = Ce, Pr, and Nd, were measured (50–60 spots on 5–8 grains). The averaged results are given in Table 10. The low values of 1σ indicate high homogeneity of the crystals. In addition, line scans were performed on needle-like crystals (30 spots per crystal), thus showing a homogeneous distribution of chlorine inside these crystals.

The totals of the analyses vary between 99% and 101%, a sign for the high quality of the analysis of light elements in a difficult matrix. They also indicate that the standards for the light elements N and O were a suitable choice. It is important to note that, despite the difficulties known for light element EPMA analysis in non-conductive samples [26], the analysis of N and O in the oxonitridosilicate chlorides is possible with high precision and accuracy.

The pure $Ce_3Si_6N_{11}$ and $Pr_3Si_6N_{11}$ standards show a low oxygen content of 0.2 wt% (Table 10). The small peak at the oxygen $K\alpha$ line cannot be assigned to an overlapping rare-earth element line. The oxygen peak may rather be due to a thin oxygen-bearing surface layer, since crystal structure refinement indicates no oxygen dissolved in the bulk crystal [14]. The small amount was therefore neglected for the structural formula calculation. In the other samples, there may also be an additional small oxygen content due to such oxygen-bearing surface layers which would slightly increase the sum of the analyses.

4. Conclusions

The simultaneous substitution of oxygen with chlorine and nitrogen leads to an interesting class of new compounds, being characterized by the existence of complex cations $[ClLn_4]^{n+}$. The use of a wide scope of different methods is required to understand such complex structures and the nature of the diverse possibilities of substitution (Cl/O-, N/O-, Ln-substitution).

Taking into account the results of the different methods a range of compositional homogeneity of the oxonitridosilicate chlorides is assumed and will be investigated. So far, for the chlorine compound we have synthesized and analyzed (EPMA) two samples with different chlorine content and investigated their high-pressure behavior [27].

The substitutional effects on the material properties (e.g., hardness, thermal stability, spectroscopic behavior under high pressure) of these compounds are subject of current investigations and will be published in a forthcoming paper. Special interest will be given to the high-pressure behavior, where a postulated phase transition [9] could be observed and will be investigated further by synchrotron single-crystal diffraction and by spectroscopic methods.

Table 10
Quantitative results of the EPMA analyses

		Si	Pr	Ce	Cl	N	Nd	O	Total	No. of spots
$Ce_4[Si_4O_{3+x}N_{7-x}]Cl_{1-x}O_x$										60
wt%	Average	13.25	0	66.33	3.59	11.43	0	5.91	100.49	
	1σ	0.09	0	0.22	0.09	0.12	0	0.13	0.42	
Atomic ratio	Average	21.14	0	21.22	4.53	36.57	0	16.54	100	
	1σ	0.10	0	0.11	0.14	0.21	0	0.28		
Stoichiom. formula		3.99		4.01	0.86	6.91		3.12	18.89	
$Pr_4[Si_4O_{3+x}N_{7-x}]Cl_{1-x}O_x$										59
wt%	Average	13.19	64.72	0	3.51	11.46	0	5.93	98.81	
	1σ	0.09	0.11	0	0.06	0.15	0	0.08	0.3	
Atomic ratio	Average	21.19	20.72	0	4.47	36.91	0	16.71	100	
	1σ	0.17	0.13	0	0.08	0.25	0	0.18		
Stoichiom. formula		4.04	3.95		0.85	7.03		3.18	19.05	
$Nd_4[Si_4O_{3+x}N_{7-x}]Cl_{1-x}O_x$										50
wt%	Average	13.16	0	0.05	3.79	11.42	66.48	5.59	100.49	
	1σ	0.05	0	0.01	0.03	0.11	0.1	0.05	0.16	
Atomic ratio	Average	21.28	0	0.02	4.86	37.04	20.95	15.86	100	
	1σ	0.1	0	0	0.04	0.2	0.1	0.11		
Stoichiom. formula		4.03			0.92	7.02	3.97	3.00	18.94	
$Ce_3Si_6N_{11}$										3
wt%	Average	22.36	0	56.66	0.01	20.78	—	0.24	100.1	
	1σ	0.17	0	0.19	0.00	0.14	—	0.01	0.21	
Atomic ratio	Average	29.49	0	14.98	0.01	54.96	—	0.56	100.00	
	1σ	0.23	0	0.07	0.00	0.32	—	0.03		
Stoichiom. formula		5.95		3.03		11.10		0.11	20.19	
$Pr_3Si_6N_{11}$										3
wt%	Average	22.49	56.66	0	0	21.28	—	0.17	100.60	
	1σ	0.11	0.07	0	0	0.18	—	0.02	0.37	
Atomic ratio	Average	29.29	14.72	0	0	55.59	—	0.40	100.00	
	1σ	0.07	0.08	0	0	0.13	—	0.05		
Stoichiom. formula		5.99	3.01			11.36		0.08	20.44	

Acknowledgments

The authors would like to thank the Deutsche Forschungsgemeinschaft (SPP 1136 "Substitutionseffekte in Festkörpern", Projekt SCHN 377/9) and the Fonds der Chemischen Industrie for generous financial support. Thanks are given to Cora Hecht (LMU München, Germany) for preparing the sample for the powder neutron diffraction measurement. We would also like to acknowledge the help of Dr. Konstantin Klementiev at the beamline E4 (HASYLAB/DESY).

References

[1] W. Schnick, H. Huppertz, Chem. Eur. J. 3 (1997) 679.
[2] W. Schnick, T. Schlieper, H. Huppertz, K. Köllisch, M. Orth, R. Bettenhausen, B. Schwarze, R. Lauterbach, Phosphorus Sulfur 124/125 (1997) 163.
[3] E. Irran, K. Köllisch, S. Leoni, R. Nesper, P.F. Henry, M.T. Weller, W. Schnick, Chem. Eur. J. 6 (2000) 2714.
[4] F. Liebau, Structural Chemistry of Silicates, Springer, Berlin, 1985.
[5] S.V. Krivovichev, S.K. Filatov, T.F. Semenova, Russ. Chem. Rev. 67 (1998) 137.
[6] G. Meyer, T. Schleid, Z. Anorg. Allg. Chem. 528 (1985) 55.
[7] S.A. Hodorowicz, M. Olejak-Chodan, H.A. Eick, J. Solid State Chem. 71 (1987) 205.
[8] F. Lissner, T. Schleid, Z. Anorg. Allg. Chem. 624 (1998) 1903.
[9] B. Winkler, M. Hytha, U. Hantsch, V. Milman, Chem. Phys. Lett. 343 (2001) 622.
[10] W. Schnick, H. Huppertz, R. Lauterbach, J. Mater. Chem. 9 (1999) 289.
[11] H. Lange, G. Wötting, G. Winter, Angew. Chem. Int. Ed. Engl. 30 (1991) 1579.
[12] T. Schlieper, W. Schnick, Z. Kristallogr. 211 (1996) 254.
[13] M. Woike, W. Jeitschko, Inorg. Chem 34 (1995) 5105.
[14] T. Schlieper, W. Schnick, Z. Anorg. Allg. Chem. 621 (1995) 1535.
[15] G.M. Sheldrick, SHELXS97, Program for the Solution of Crystal Structures and SHELXL97, Program for the Refinement of Crystal Structures, University of Göttingen, 1997.
[16] R.B. Von Dreele, A.C. Larson, Programm GSAS General Structure Analysis System, Los Alamos National Laboratory, Los Alamos, 2001.
[17] J.T. Armstrong, Caltech 1993, Jeol License of CITZAF Version 3.5.
[18] G.F. Bastin, H.J.M. Heijligers, Quantitative electron probe microanalysis of nitrogen, Internal Report, Eindhoven University of Technology, 1988.

[19] G.F. Bastin, H.J.M. Heijligers, Quantitative electron probe microanalysis of oxygen, Internal Report, Eindhoven University of Technology, 1989.
[20] A.V. McGuire, C.A. Francis, M. Darby Dyar, Am. Miner. 77 (1992) 1087.
[21] E. Jarosewich, J.A. Nelen, J.A. Norberg, Geostandards Newslett. 4 (1980) 43.
[22] E. Jarosewich, Geostandards Newslett. 15 (1991) 397.
[23] H. Lueken, Magnetochemie, Teubner, Stuttgart, 1999.
[24] G. Kotzyba, R. Mishra, R. Pöttgen, Z. Naturforsch. 58b (2003) 497.
[25] G. Kaindl, G.K. Wertheim, G. Schmiester, E.V. Sampathkumaran, Phys. Rev. Lett. 58 (1987) 606.
[26] G.F. Bastin, H.J.M. Heijligers, in: K.F.J. Heinrich, D.E. Newbury (Eds.), Electron Probe Quantitation, Plenum Press, New York, 1991, p. 163.
[27] A. Friedrich, K. Knorr, A. Lieb, S. Rath, M. Hanfland, B. Winkler, W. Schnick, Z. Kristallogr, in press.